Fixed and mobile energy storage coordination optimization method for enhancing photovoltaic integration capacity considering voltage offset

Liang Feng[1], Ni Jianfu[1], Yu Zhuofei[1], Zhang Kun[2,3]*, Zhao Qianyu[2,3] and Wang Shouxiang[2,3]

[1]Grid Electric Power Research Institute Corporation, Nari Group Corporation State, Nanjing, Jiangsu, China, [2]Tianjin Key Laboratory of Power System Simulation Control, Tianjin, China, [3]Key Laboratory of Smart Grid of Ministry of Education (Tianjin University), Tianjin, China

Mobile energy storage has the characteristics of strong flexibility, wide application, *etc.*, with fixed energy storage can effectively deal with the future large-scale photovoltaic as well as electric vehicles and other fluctuating load access to the grid resulting in the imbalance of supply and demand. To this end, this paper proposes a coordinated two-layer optimization strategy for fixed and mobile energy storage that takes into account voltage offsets, in the context of improving the demand for local PV consumption. Among them, the upper layer optimization model takes into account the minimum operating cost of fixed and mobile energy storage, and the lower layer optimization model minimizes the voltage offset through the 24-h optimal scheduling of fixed and mobile energy storage in order to improve the *in-situ* PV consumption capacity. In addition, considering the multidimensional nonlinear characteristics of the model, the interaction force of particles in the Universe is introduced, and the hybrid particle swarm-gravitational search algorithm (PSO-GSA) is proposed to solve the model, which is a combination of the individual optimization of the particle swarm algorithm and the local search capability of the gravitational search algorithm, which improves the algorithm's optimization accuracy. Finally, the feasibility and effectiveness of the proposed model and method are verified by simulation analysis with IEEE 33 nodes.

KEYWORDS

distribution grids, photovoltaic local consumption, fixed energy storage systems, mobile energy storage systems, energy storage scheduling strategies, hybrid particle swarmgravitational search algorithms

1 Introduction

With the large-scale integration and increasing penetration rate of distributed energy sources, the stochastic, intermittent, and fluctuating nature of their outputs constrains the absorptive capacity of the distribution network. Energy storage systems, leveraging their flexible energy management capabilities and rapid power regulation capabilities, can address issues such as wind and solar power curtailment, voltage violations, and insufficient peak shaving capacity in the distribution network. Properly configuring

energy storage systems is of paramount importance for the efficient operation of the distribution network (Wang et al., 2014; Wang et al., 2021).

In recent years, scholars both domestically and internationally have conducted research on grid energy storage optimization strategies to facilitate the integration of renewable energy. In the realm of fixed energy storage systems, Fixed Energy Storage Systems (FESS), literature (Shi et al., 2021) establishes a joint configuration model for solar and storage with the objective of optimizing photovoltaic integration and system economy. Literature (Zhou et al., 2016), considering the impact of solar and storage as well as demand response, develops a microgrid investment profit model with the goals of optimizing photovoltaic utilization and operational economy. Literature (Pasetti et al., 2021) indicates that as the capacity and quantity of energy storage systems increase, they become susceptible to network attacks. Application of Man-in-the-Middle (MitM) attacks on BESS can decrease the lifespan of storage, lead to economic losses, and affect the security and stability of the power grid. Collaboration with Distribution System Operators (DSOs) through increased cross-checks is proposed as a preventive measure. Literature (Morstyn et al., 2018) reviews the progress of microgrid energy storage coordination control strategies and proposes a distributed intelligent microgrid control framework based on intelligent agent networks. The framework aims to provide a universally applicable control strategy for the development of intelligent decentralized power grids, offering insights into the future development of distribution networks. Literature (Lu et al., 2023) presents a dual-layer optimization model for the rapid recovery of EMS distribution systems. The upper layer minimizes system load shedding rate from a scheduling perspective, while the lower layer addresses post-disaster economic dispatch issues through Karush-Kuhn-Tucker (KKT) simplification into a single-layer mixed-integer linear programming problem. Focusing on flexible switchgear in AC/DC distribution networks, literature (Ma et al., 2023) considers equipment constraints, peak shaving, and voltage deviation constraints to build a real and reactive power dispatch model with the minimum operating cost as the primary objective. Through the construction of a two-stage stochastic-distributionally robust optimization model, solar output variability is simulated. Literature (Wei et al., 2023) proposes a flexible interconnection distribution network optimization and control strategy considering transformer and SOP loss characteristics. A dual-layer model is established with the upper layer aiming for the lowest annual comprehensive cost and the lower layer seeking the lowest comprehensive loss. Considering intelligent topology changes, literature (Pan et al., 2023) introduces a consistency algorithm and establishes a SOP cluster control model for distribution networks. Through an SOP cluster strategy based on the consistency algorithm, global SOP collaborative optimization is achieved, enhancing the balance of distribution network feeders. Literature (Liu et al., 2023) presents a dual-layer planning method for distributed power sources and generalized energy storage. The upper layer addresses location and capacity decisions considering system planning costs and response incentives, while the lower layer uses an adaptive parameter particle swarm optimization algorithm to solve the optimization problem based on the continuity and reliability of the distribution network. Literature (Yang et al., 2022) introduces a

multi-objective dual-layer structure for energy storage systems. The inner layer aims to maximize operational revenue using the peafowl optimization algorithm, while the outer layer targets minimum operation and maintenance costs, minimum voltage fluctuation, and minimum load fluctuation using the multi-objective peafowl optimization algorithm. Literature (Mao et al., 2019) introduces a dual-layer optimization for generalized energy storage configuration, with the upper layer utilizing a genetic algorithm for energy storage configuration and the lower layer obtaining optimal energy storage operation using dynamic programming. In the aforementioned studies, joint planning of energy storage primarily focuses on the reliability and economic viability on the grid side, yet there is a lack of research on the impact of the uncertainty of distributed energy source outputs on energy storage planning and the optimization of distribution network operation.

Mobile Energy Storage Systems (MESS) are primarily composed of energy storage devices and mobile equipment. Compared to fixed energy storage, MESS can flexibly select access points and capacities based on load characteristics, reducing daily maintenance costs, peak shaving, and enhancing the flexibility of the distribution network. Literature (Astero et al., 2017) indirectly controls photovoltaic integration through electricity prices for electric vehicles. Literature (Kwon et al., 2020) establishes two-stage mobile energy storage optimization models. Literature (Abdeltawab and Mohamed, 2017) considers the fuel costs of mobile energy storage vehicles and the full lifecycle of energy storage. Literature (Yao et al., 2020) utilizes mobile energy storage as a backup power source for natural disasters or emergency situations. In summary, MESS possesses both mobility and energy storage functions, allowing flexible selection of access points and capacities based on grid operating conditions. This capability can effectively avoid redundant waste, reduce daily maintenance costs, and significantly improve the economic viability of peak shaving. However, its drawback lies in its smaller capacity. MESS can complement fixed energy storage, jointly participating in grid regulation. Through real-time monitoring of power system operations, rational control of both BESS and MESS is crucial for improving load characteristics (Chen et al., 2016).

This paper integrates FESS and MESS collaborative optimization methods, proposing energy storage configuration and operation strategies to enhance photovoltaic absorption capacity in extreme scenarios. Both upper and lower layers adopt an improved Particle Swarm Optimization-Gravitational Search Algorithm (PSO-GSA) method, combining the individual optimization capability of the particle swarm algorithm with the local search capability of the gravitational search algorithm to enhance global search capability. In the upper layer, decision variables include fixed energy storage site selection, capacity, and mobile energy storage access nodes and capacity, comprehensively considering the economic operation of FESS and MESS. The lower layer dynamically optimizes energy storage charging and discharging strategies with the objective of minimizing grid voltage deviation. In extreme photovoltaic scenarios, the goal is to enhance on-site photovoltaic absorption capacity and improve grid operation conditions.

2 Distribution network component model

2.1 Photovoltaic penetration rate definition

Photovoltaic penetration rate is defined as the ratio of the maximum photovoltaic output power to the maximum load output power:

$$D_{PV} = \frac{F_{MAX}}{F_{L,MAX}} \times 100\% \tag{1}$$

In the formula 1: D_{PV} represents the photovoltaic penetration rate; F_{MAX} represents the maximum photovoltaic output power; $F_{L,MAX}$ represents the maximum load output power.

People have different criteria for judging the level of photovoltaic penetration. Generally, when it is below 20%, it is considered a low-penetration stage, where the scale of photovoltaic integration into the grid is small, and its impact on the power grid is minimal. As the penetration of photovoltaics increases, when the photovoltaic penetration rate reaches 20%–80%, it becomes necessary to address the issue of enhancing the carrying capacity of photovoltaics in concentrated areas. At this stage, the significant integration of photovoltaics may lead to power reverse flow in the power system. When the photovoltaic penetration rate exceeds 100%, it can be considered a high-penetration stage. At this point, there is a substantial reverse flow of photovoltaic power into the power system, and the role of photovoltaic energy shifts to the supply side. The difficulty of on-site absorption of photovoltaics increases, requiring interventions such as energy storage to enhance the capacity for photovoltaic integration.

2.2 Photovoltaic on-site absorption rate definition

The on-site absorption of photovoltaic power is primarily influenced by the load and energy storage. In this paper, we define the on-site absorption rate of photovoltaic power as:

$$\varphi = \sum_{t=6}^{19} \left(\frac{P_{PV,fact,t} - P_{LOAD,t} - P_{ESS,t}}{P_{PV,fact,t}} \right) \times 100\% \tag{2}$$

In the formula 2: Where φ represents the on-site absorption rate of photovoltaic power; $P_{PV,fact,t}$ represents the actual generation of photovoltaics at time t. $P_{LOAD,T}$ represents the distribution network load during the photovoltaic generation period at time t, and $P_{ESS,t}$ represents the load for energy storage charging during the photovoltaic generation period at time t.

2.3 Distributed power generation model

2.3.1 Photovoltaic output model

The photovoltaic generation intensity is controlled by the regional solar irradiance. Solar irradiance is commonly considered to follow a Beta distribution, where the Beta probability density function is given by:

$$\mathbf{f}(r) = \frac{\Gamma(\alpha + \beta)}{\Gamma(\alpha)\Gamma(\beta)} \left(\frac{r}{r_{max}} \right)^{\alpha-1} \left(1 - \frac{r}{r_{max}} \right)^{\beta-1} \tag{3}$$

In the formula 3: Where α and β are the shape parameters of the Beta distribution; r is the actual solar irradiance during a specific time period, and r_{max} is the maximum solar irradiance during that time period. Research indicates that the output power of photovoltaic generation is influenced by solar irradiance, photovoltaic panel area, and photovoltaic conversion efficiency. Therefore, the relationship between the output power of photovoltaic generation and solar irradiance is given by:

$$P_s = rMA\eta \tag{4}$$

$$\mathbf{f}(r) = \frac{\Gamma(\alpha + \beta)}{\Gamma(\alpha)\Gamma(\beta)} \left(\frac{P_S}{r_{max}A\eta} \right)^{\alpha-1} \left(1 - \frac{P_S}{r_{max}A\eta} \right)^{\beta-1} \tag{5}$$

In the formulas 4, 5: Where P_s represents the photovoltaic output power; A is the photovoltaic panel area; η is the photovoltaic conversion efficiency.

2.3.2 Fixed energy storage model

The charging and discharging model for fixed energy storage is as follows:

$$\begin{cases} P_{ES,j}(t) \le 0, ES_j(t) = ES_j(t-1)(1-\delta) + P_{ES,j}(t)\eta_c \Delta t \\ P_{ES,j}(t) > 0, ES_j(t) = ES_j(t-1)(1-\delta) - \dfrac{P_{ES,j}(t)\Delta t}{\eta_d} \\ \sum\limits_{t=1}^{T} \left[P_{ES,j}(t)a_1\eta_c + P_{ES,j}(t)\dfrac{a_2}{\eta_d} \right] \Delta t = 0 \end{cases} \tag{6}$$

In the formula 6: Where $P_{ES,j}(t) \le 0$ represents energy storage charging, η_c represents the charging efficiency of energy storage, and in this case $a_1 = 1, a_2 = 0$; $P_{ES,j}(t) > 0$ represents energy storage discharging, η_d represents the discharging efficiency of energy storage, and in this case $a_1 = 0, a_2 = 1$.

2.3.3 Mobile energy storage model

The charging and discharging model for mobile energy storage is as follows:

$$-P_N \le P_{i,t}^{MES} \le P_N \tag{7}$$

$$E_{t+1}^{MES} = E_t^{MES} - P_{i,t}^{MES}\Delta t \tag{8}$$

$$E_{min}^{MES} \le E_t^{MES} \le E_{max}^{MES} \tag{9}$$

$$E_0^{MES} = E_T^{MES} \tag{10}$$

In the formulas 7–10: Where P_N represents the rated power of mobile energy storage; $P_{i,t}^{MES}$ represents the injected power at node i by mobile energy storage at time t; E_t^{MES} represents the state of charge of mobile energy storage at time t; E_{min}^{MES} and E_{max}^{MES} are the maximum and minimum values of the state of charge of mobile energy storage, respectively; E_0^{MES} and E_T^{MES} are the state of charge of mobile energy storage at the beginning and end of the operating cycle, respectively.

2.4 Electric vehicle charging model

Monte Carlo sampling is used to analyze the electric vehicle charging model.
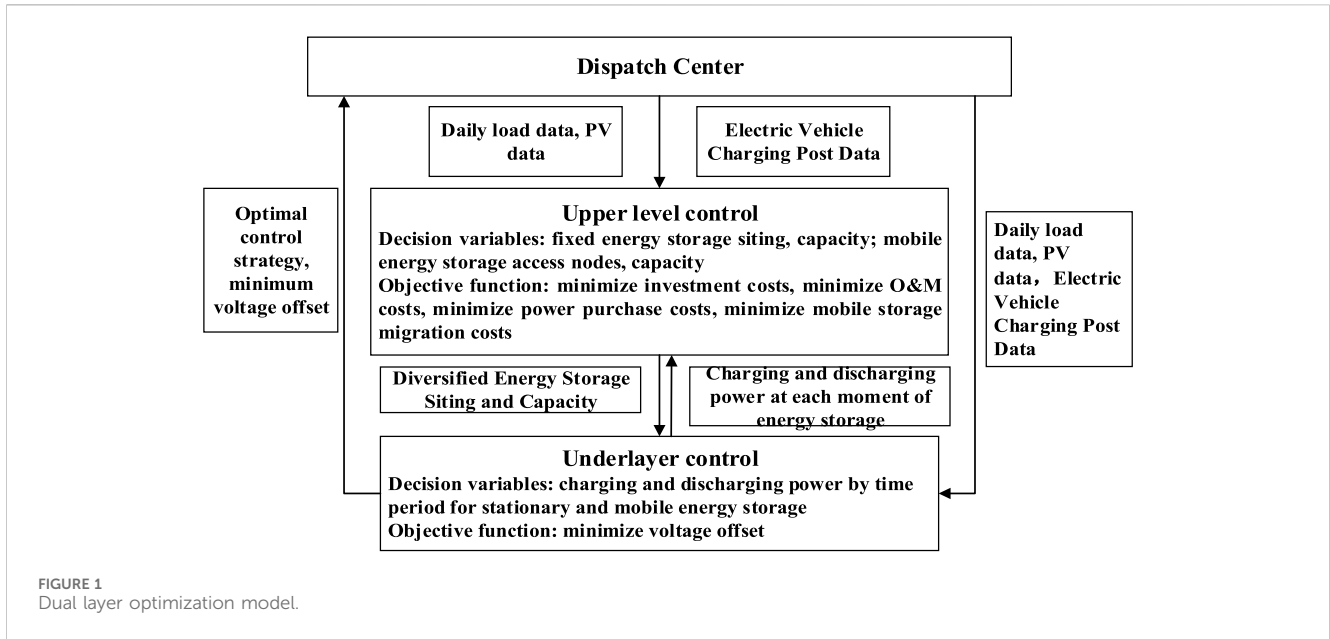
FIGURE 1
Dual layer optimization model.

(1)Probability Distribution of Daily Driving Distance

Processing behavioral data on electric vehicle usage, it is determined that the daily driving distance follows a log-normal distribution, i.e.,:

$$f_s(x) = \frac{1}{x} \frac{1}{\sqrt{2\pi}} \exp\left(-\frac{(\ln x - \mu_s)^2}{2\sigma_s^2}\right) \qquad (11)$$

In the formula 11: Where μ_s taking the mean as 3.2 and σ_s the variance as 0.88.

(2)Probability Distribution of Initial Charging Time

The charging time of electric vehicles $f_t(x)$ follows a normal distribution, i.e.,:

$$f_t(x) = \begin{cases} \dfrac{1}{\sigma_s}\dfrac{1}{\sqrt{2\pi}}\exp\left(-\dfrac{(x-\mu_s)^2}{2\sigma_s^2}\right), & (\mu_s - 12 < x < 24) \\[3mm] \dfrac{1}{\sigma_s}\dfrac{1}{\sqrt{2\pi}}\exp\left(-\dfrac{(x+24-\mu_s)^2}{2\sigma_s^2}\right), & (0 < x < \mu_s - 12) \end{cases} \qquad (12)$$

In the formula 12: Where μ_s taking the mean as 17.6 and σ_s the variance as 3.4.

3 Construction of dual-layer optimization model in electrical engineering terminology

The dual-layer optimization model as shown in Figure 1.

The upper-layer optimization model has decision variables for fixed energy storage location, capacity, and mobile energy storage access nodes and capacity. The optimization objectives include minimizing investment costs, operating costs, power purchase costs, and mobile energy storage migration costs. The constraints involve energy storage output constraints and grid power purchase constraints.

The lower-layer optimization model has decision variables for the charging and discharging power of fixed and mobile energy storage during different time periods. The optimization objective is to minimize voltage offset. Constraints include voltage amplitude constraints, distributed renewable energy output constraints, and power balance constraints.

The dispatch center inputs photovoltaic data, daily load data, and electric vehicle charging station data. The upper layer solves the model to minimize operating costs, and the location and capacity of energy storage are passed as parameters to the lower layer. The lower layer controls the charging and discharging power of energy storage at each moment to minimize voltage offset. Iterations are performed until the optimal control strategy is obtained.

3.1 Upper-layer objective function

The upper layer involves multi-energy storage optimization configuration, with the objective function being the minimization of equipment investment costs, equipment operating costs, and grid power purchase costs.

$$f_{up} = w_1 \times f_1 + w_2 \times f_2 + w_3 \times f_3 + w_4 \times f_4 \qquad (13)$$

In the formula 13: Where f_1 represents equipment investment costs; f_2 represents equipment operating costs; f_3 is the grid power purchase cost; f_4 represents the cost of mobile energy storage migration; w_1、w_2、w_3、w_4 is a random number between 0 and 1, and $w_1 + w_2 + w_3 + w_4 = 1$.

(1) Minimize equipment investment costs

The equipment investment cost includes one-time investment costs for both energy storage devices and photovoltaic equipment.

$$\begin{cases} f_1 = Q\sum_{z=1}^{Z} N_z C_z \\ Q = \dfrac{q(1+q)^y}{(1+q)^y - 1} \end{cases} \qquad (14)$$

In the formula 14: Q represents the capital recovery factor; q represents the annual interest rate; Z represents equipment type; C_z represents the investment cost of equipment type Z; N_z represents the number of equipment type Z.

(2) Minimize equipment operating costs

The operating cost of equipment refers to the costs associated with regular maintenance and repair of equipment damage.

$$f_2 = \sum_{t=1}^{T}\sum_{z=1}^{Z} C_z^{loss} t + A \qquad (15)$$

In the formula 15: C_z^{loss} represents the daily operational maintenance cost of equipment z; A represents the cost of repairing equipment damage, where t is the operating time.

(3) Minimize grid power purchase costs

$$f_3 = \sum_{t=1}^{24} P_t^{line} w_t^{line} \qquad (16)$$

In the formula 16: P_t^{line} represents the power purchased from the grid at time t, and w_t^{line} represents the electricity price at time t.

(4) Minimize the cost of relocating mobile energy storage

$$f_4 = \sum_{t=1}^{24} C_{FUEL} O_{DISTANCE} \qquad (17)$$

In the formula 17: Where f_4 represents the cost of relocating mobile energy storage; C_{FUEL} represents the unit distance cost, and $O_{DISTANCE}$ represents the distance traveled by the energy storage vehicle.

3.2 Upper-layer objective constraints

(1) Energy Storage Output Constraint.

$$\begin{cases} P_{ES,j}^{\min} \leq P_{ES,j}(t) \leq P_{ES,j}^{\max} \\ 0.2 \leq SOC_j(t) \leq 0.9 \\ SOC_j(0) = 0.5 \end{cases} \qquad (18)$$

In the formula 18: Where $P_{ES,j}^{\min}$ represents the lower limit of the charging or discharging power for the jth energy storage unit, $P_{ES,j}(t)$ represents the charging or discharging power of the jth energy storage unit at time t, $P_{ES,j}^{\max}$ represents the upper limit of the charging or discharging power for the jth energy storage unit, and $SOC_j(t)$ represents the state of charge of the energy storage at time t, with a range from 0.2 to 0.9. When t is zero, the initial state of charge $SOC_j(0)$ is set to 0.5.

(2) Electricity Purchasing Power Constraint

$$P_{t,buy} \geq 0 \qquad (19)$$

In the formula 19: Where $P_{t,buy}$ represents the electricity purchasing power.

3.3 Lower-level objective function

The lower level involves 24-h economic dispatch of the distribution network, with the minimization of voltage deviation as the objective function.

In power systems, voltage difference reflects the operational safety of the distribution network, as excessive voltage deviation can impact the operation of electrical equipment and the quality of electrical energy.

$$f_{low} = \sum_{t=1}^{24}\left(\sum_{i=1}^{N}\left(\frac{\Delta U_{i,t}}{U_{i,\max} - U_{i,\min}}\right)^2\right) \qquad (20)$$

$$\Delta U_{i,t} = \begin{cases} U_{i,\min} - U_{i,t}, U_{i,t} < U_{i,\min} \\ 0, U_{i,\min} \leq U_{i,t} \leq U_{i,\max} \\ U_{i,t} - U_{i,\max}, U_{i,t} \geq U_{i,\max} \end{cases} \qquad (21)$$

In the formulas 20, 21: Where $\Delta U_{i,t}$ represents the voltage deviation at time t, $U_{i,t}$ represents the voltage at node i at time t, and $U_{i,\min}$, $U_{i,\max}$ represent the upper and lower limits of node i, respectively. In medium and low voltage distribution networks, the permissible range for voltage deviation is −5% to +5%.

3.4 Lower-level objective constraints

(1) Voltage magnitude constraints

$$U_{i,\min} \leq U_{i,t} \leq U_{i,\max} \qquad (22)$$

In the formula 22: Where $U_{i,\min}$ represents the voltage lower limit at node i, U_i represents the voltage at node i, and $U_{i,\max}$ represents the voltage upper limit at node i.

(2) Distributed New Energy Output Constraint

$$P_{pv,\min} \leq P_{pv}^t \leq P_{pv,\max} \qquad (23)$$

In the formula 23: Where $P_{pv,\min}$ represents the minimum output of photovoltaic power, P_{pv}^t represents the photovoltaic power output at time t, and $P_{pv,\max}$ represents the maximum output of photovoltaic or wind power.

(3) Power Balance Constraint

$$\begin{cases} P_{s,i} - P_{L,i} = U_i \sum_{j=1}^{n} U_j \left(G_{ij}\cos\theta_{ij} + B_{ij}\sin\theta_{ij}\right) \\ Q_{s,i} - Q_{L,i} = U_i \sum_{j=1}^{n} U_j \left(G_{ij}\sin\theta_{ij} - B_{ij}\cos\theta_{ij}\right) \end{cases} \qquad (24)$$

In the equation 24: $P_{s,i}$ represents the active power output at node i due to the power source; $P_{L,i}$ represents the active power output of the load at node i; U_i represents the voltage at node i; U_j represents the voltage at node j; $Q_{s,i}$ represents the reactive power output at node i due to the power source; $Q_{L,i}$ represents the reactive power output of the load at node i.

4 Optimization solving algorithm based on PSO-GSA

The ultimate goal of heuristic algorithms is global optimization. To achieve this goal, the exploratory and exploitative capabilities of heuristic algorithms are particularly crucial.

4.1 Particle swarm algorithm

The particle swarm algorithm (Anantathanavit and Munlin, 2013) models each particle considering the current velocity, current position, and a distance-modifying function to pbest and gbest as follows.

$$v_i^{t+1} = wv_i^t + c_1 \times rand \times \left(pbest_i^t - x_i^t \right) + c_2 \times rand \times \left(gbest - x_i^t \right) \tag{25}$$

In the equation 25: w represents the weighted function; v_i^t represents the velocity of the i th particle at generation t; c_1 represents the weighting factor; $rand$ is a random number between 0 and 1; $pbest_i^t$ represents the best position of the particle at generation t; x_i^t represents the position of the particle at generation t; c_2 represents the weighting factor; $gbest$ represents the best solution. wv_i^t represents the exploration ability of the particle; $c_1 \times rand \times \left(pbest_i^t - x_i^t \right)$ represents the personal ability of the particle; $c_2 \times rand \times \left(gbest - x_i^t \right)$ represents the cooperative ability of the particle

$$x_i^{t+1} = x_i^t + v_i^{t+1} \tag{26}$$

In the formula 26: Where x_i^{t+1} represents the position of particle i at generation t+1.

4.2 Gravity search algorithm

GSA (Doraghinejad et al., 2012) originates from Newton's fundamental theory: the interaction force among particles in the Universe, a force proportional to the particle mass and inversely proportional to the distance between them, is modeled as follows.

$$F_{ij}^d(t) = G(t) \frac{M_{pi}(t) \times M_{aj}(t)}{R_{ij}(t) + \xi} \left(x_j^d(t) - x_i^d(t) \right) \tag{27}$$

In the formula 27: Where $F_{ij}^d(t)$ represents the gravitational force of particle i on particle j in the d-dimensional space at the tth iteration; $G(t)$ represents the value of universal gravitational force at the tth iteration; $M_{pi}(t)$ is the active gravitational mass; $M_{aj}(t)$ is the passive gravitational mass; $R_{ij}(t)$ represents the Euclidean distance between i and j; ξ is a constant; $x_j^d(t)$ represents the position of particle j in the d-dimensional space at the tth generation; $x_i^d(t)$ represents the position of particle i in the d-dimensional space at the tth generation.

$$G(t) = G_0 \times e^{\frac{-\partial \times iter}{\max iter}} \tag{28}$$

In the formula 28: Where ∂ represents the descent coefficient; G_0 represents the initial value; $iter$ is the current iteration number; $\max iter$ is the maximum iteration number.
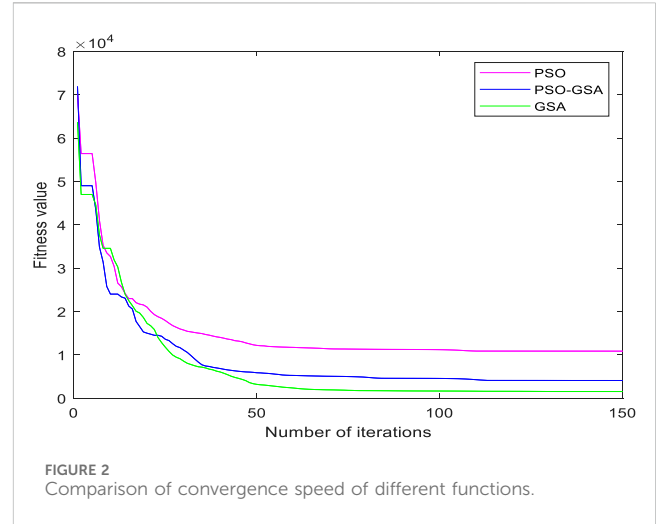

FIGURE 2
Comparison of convergence speed of different functions.

$$F_i^d(t) = \sum_{j \neq i, j \in kbest}^{N} rand_j F_{ij}^d(t) \tag{29}$$

In the formula 29: Where $F_i^d(t)$ represents the total force experienced by individual i in the d-dimensional space at the tth iteration.

$$a_i^d(t) = \frac{F_i^d(t)}{M_i(t)} \tag{30}$$

In the formula 30: Where represents $a_i^d(t)$ the equation for the acceleration of individual i in the d-dimensional space; $M_i(t)$ represents the mass of individual i at generation t.

$$v_i^d(t+1) = rand \times v_i^d(t) + a_i^d(t) \tag{31}$$

In the formula 31: Where $v_i^d(t+1)$ represents the velocity of particle i in the d-dimensional space at generation t+1.

$$x_i^d(t+1) = x_i^d(t) + v_i^d(t+1) \tag{32}$$

In the formula 32: Where $x_i^d(t+1)$ represents the position of particle i in the d-dimensional space at generation t+1.

4.3 PSO-GSA hybrid algorithm

The PSO-GSA hybrid algorithm combines the individual optimization capability of PSO with the local search ability of GSA such as the formulas 33, 34. The improved convergence of PSO-GSA surpasses that of standalone PSO and GSA.

$$v_i^{t+1} = wv_i^t + c_1 \times rand \times a_i^t + c_2 \times rand \times \left(gbest - x_i^t \right) \tag{33}$$

$$x_i^{t+1} = x_i^t + v_i^{t+1} \tag{34}$$

Initially, each particle is considered to have a candidate solution. After initialization, the gravitational force, gravitational constant, and resultant force between particles are calculated. During the iteration process, the algorithm updates to the current best solution, computes the velocity of
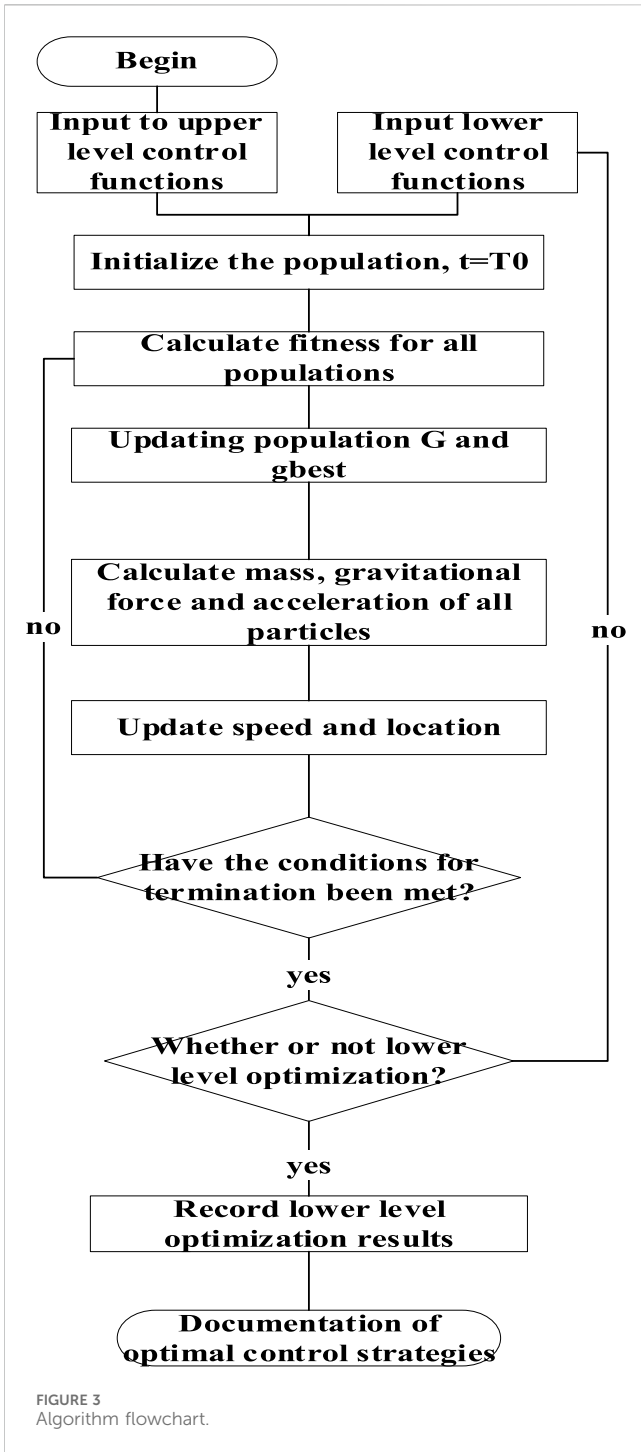
FIGURE 3
Algorithm flowchart.

FIGURE 4
IEEE 33 node distribution network.
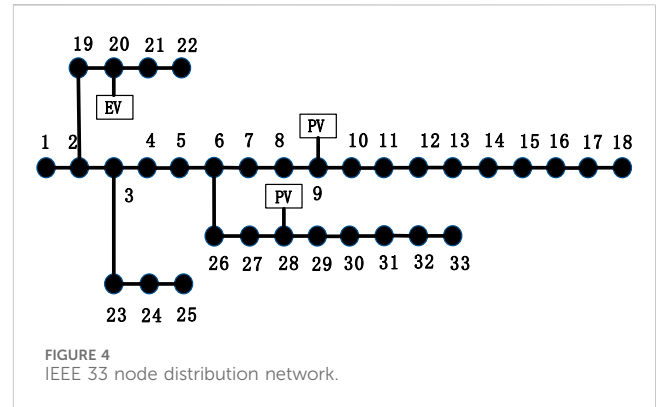
5 Case analysis

5.1 Case parameters

Simulations were conducted on the IEEE 33-node distribution network using Matlab 2021a software. The system's base voltage is 12.66 kV, and the maximum load is 3.715 MW. To provide reserve capacity for photovoltaic integration at system nodes, the upper limit of node voltage is set to 1.05, and the lower limit is set to 0.95. Photovoltaic panels are integrated at nodes 9 and 28, while an electric vehicle charging station is added at node 20, as illustrated in Figure 4.

Monte Carlo simulations were employed to model the starting density and charging power of electric vehicles, with a total of 2000 vehicles. The simulation results are presented in Appendix Figure A1 and Figure A2.

This study focuses primarily on the impact of the fixed and mobile energy storage access points and capacities on the integration of photovoltaics. The basic information for both fixed and mobile energy storage is as follows: the energy storage maintenance coefficient is 0.02; the unit capacity investment cost is 1000 CNY/KW; the discount rate is 0.08; the service life is 20 years. For mobile energy storage, the cost per kilometer varies based on the distance traveled each time, and here it is calculated at a monthly cost of 3,000 Yuan. The energy storage electricity prices are 0.31 CNY/kWh from 0:00 to 8:00, 0.84 CNY/kWh from 9:00 to 11:00, 0.31 CNY/kWh from 12:00 to 13:00, 0.84 CNY/kWh from 14:00 to 21:00, and 0.31 CNY/kWh from 22:00 to 24:00.

To achieve coordinated optimization of fixed and mobile energy storage for enhancing the distribution network's consumption capacity, a PSO-GSA hybrid algorithm is applied to both the upper-layer multi-energy storage optimization configuration and the lower-layer energy storage optimization scheduling. The fixed energy storage locations range from node 2 to 33, with capacities from 0.5 MW to 1 MW. The access nodes for mobile energy storage range from node 2 to 33 (assuming node 1 is the reference node), with capacities from 0.4 MW to 0.9 MW. Fixed energy storage charges during off-peak hours or when photovoltaic energy cannot be accommodated and discharges during peak electricity demand. In contrast, mobile energy storage offers more flexible charge and discharge regulation, responding dynamically to real-time situations in case of emergencies or when fixed energy storage cannot effectively regulate. The PSO-GSA hybrid algorithm is applied to both upper and lower layers with 50 particles each, 50 iterations, an individual learning factor of 0.5, and a global learning factor of 1.5.

particles for the (n+1)-th generation, and finally updates the positions of the particles.

The improved convergence of PSO-GSA is superior to that of PSO and GSA, as shown in Figure 2.

4.4 The Flowchart of the PSO-GSA Algorithm.

The flow chart of the PSO-GSA algorithm is shown in Figure 3.

TABLE 1 Energy storage parameters.

Scenes	Fixed energy storage, mobile energy storage access location	Fixed energy storage, mobile energy storage access capacity/MW	Total cost of energy storage operation/ten thousand yuan	Voltage offset	Photovoltaic local consumption rate (%)
Scene 1	-	-	0	0.0082	64.39
	-	-			
Scene 2	27	0.9849	317.07	0.0072	67.40
	-	-			
Scene 3	29	0.7339	421.94	0.0064	70.16
	22	0.6096			
Scene 4	27	0.7070	419.76	0.0033	71.39
	31	0.6265			

5.2 Optimization result analysis

Firstly, without the addition of any energy storage, gradually increasing photovoltaics until the voltage exceeds the limit at nodes 9 or 28, marks the maximum photovoltaic capacity that the distribution network can bear. The maximum capacity is determined to be 2.9 MW.

Considering the future large-scale integration of photovoltaics and the transition of photovoltaic energy from the demand side to the supply side, there may be reverse power flows. In such scenarios, energy storage can be flexibly adjusted to enhance photovoltaic energy integration, reduce the risk of voltage exceeding limits, and improve the stability of the power system. When there is a sudden increase in photovoltaics and fixed energy storage devices cannot regulate effectively, flexible adjustments can be made using mobile energy storage. The following case considers an extreme photovoltaic output scenario of 2.9 MW and a charging station output of 0.6 MW.

To validate the effectiveness of the proposed model and method, a comparison is made across four different scenarios. Scenario One: integration of photovoltaics without energy storage; Scenario Two: integration of photovoltaics with optimized configuration of fixed energy storage; Scenario Three: integration of photovoltaics with coordinated optimization of fixed and mobile energy storage; Scenario Four: integration of photovoltaics, electric vehicle charging station, and coordinated optimization of fixed and mobile energy storage. The analysis includes voltage offset, multi-energy storage operating costs, and on-site photovoltaic integration rate, as shown in Table 4-1.

According to Table 1, compared to Scenario One, Scenario Two, which adds fixed energy storage, reduces the voltage offset by 0.0010 and increases the on-site photovoltaic integration rate by 3.01%. Scenario Three, with the addition of both fixed and mobile energy storage, reduces the voltage offset by 0.0018 and increases the on-site photovoltaic integration rate by 5.77% compared to Scenario One. In Scenario Four, with the addition of an electric vehicle charging station load, the voltage offset is 0.0033, the on-site photovoltaic integration rate is 71.39%. Compared to Scenario One, the voltage offset increases by 0.1638, and the curtailment rate decreases by 0.8081%. These results indicate that fixed energy storage adjustment has limitations, and through coordinated optimization of fixed and mobile energy storage, the on-site photovoltaic integration can be increased, and voltage offset can be reduced.
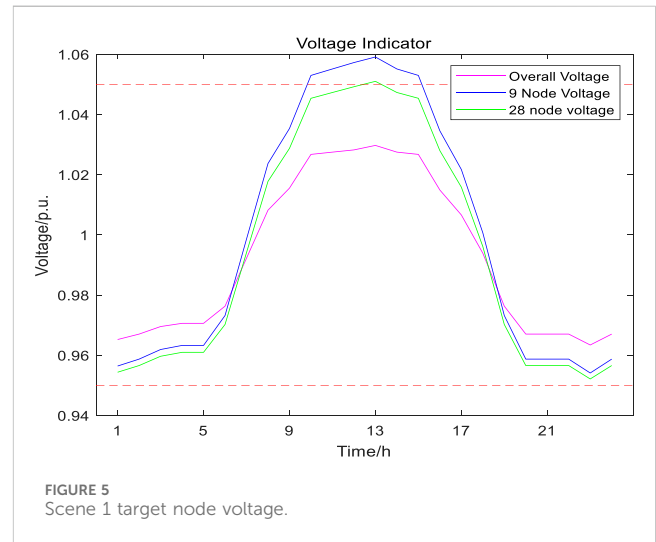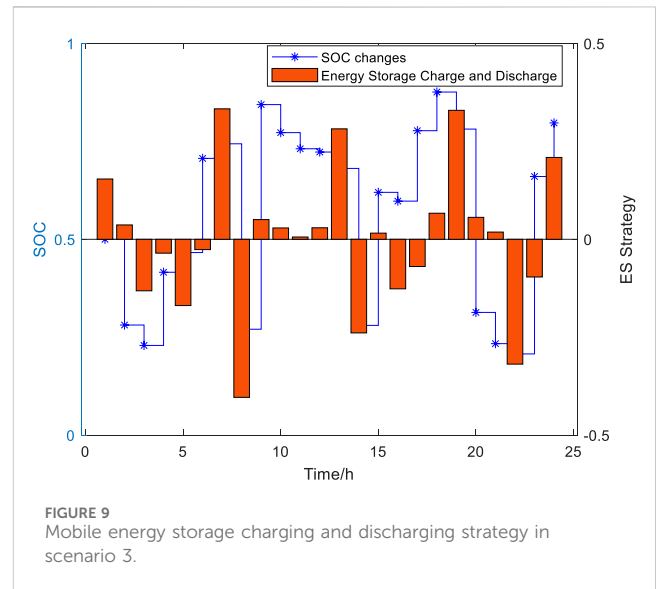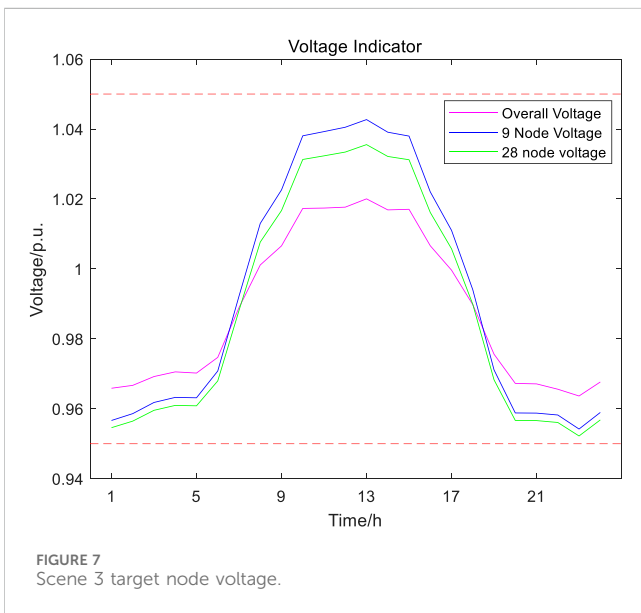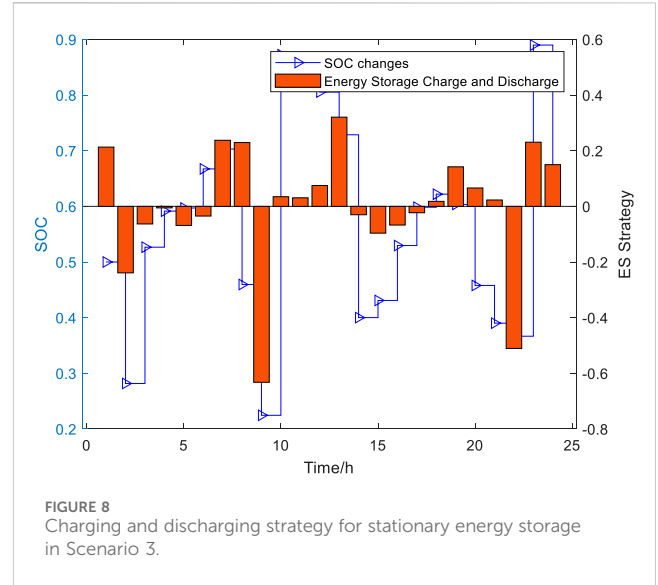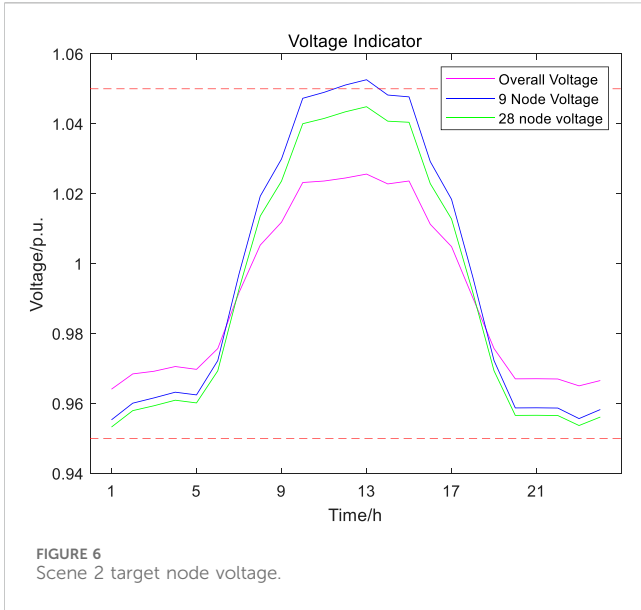

FIGURE 5
Scene 1 target node voltage.

To further illustrate the improvement in power grid stability through the coordinated optimization of fixed and mobile energy storage, a comparative analysis is conducted among Scenario One, Scenario Two, and Scenario Three.

As shown in Figure 5, Figure 6, and Figure 7, in extreme photovoltaic Scenario One, voltage exceeds the limit at nodes 9 and 28 when photovoltaics are added. From the node voltage diagram in Scenario Two, it is evident that by adding fixed energy storage, only node 9 experiences a voltage limit exceedance, and the degree of voltage offset is smaller compared to Scenario One. The node voltage diagram in Scenario Three indicates that through the coordinated action of fixed and mobile energy storage, all nodes are within the range of 0.95 p. u. to 1.05 p. u., demonstrating the efficient synergy between fixed and mobile energy storage. This synergy can significantly enhance the capacity for photovoltaic integration.

As shown in Figure 8, for the charge and discharge strategy of fixed energy storage, during 3:00–7:00 when the grid load is relatively low, the energy storage system remains in the charging state. During 10:00–14:00 when the load is high and there is sufficient photovoltaic output, fixed energy storage discharges at a lower power. From 19:00 to 22:00, when the load is high, fixed energy storage discharges, and

FIGURE 6
Scene 2 target node voltage.

FIGURE 8
Charging and discharging strategy for stationary energy storage in Scenario 3.

FIGURE 7
Scene 3 target node voltage.

FIGURE 9
Mobile energy storage charging and discharging strategy in scenario 3.

when fixed energy storage cannot meet the load requirements, coordinated operation with mobile energy storage is employed to jointly provide power support to the grid.

As illustrated in Figure 9, due to the uncertainty of photovoltaic output, there are two charging methods for the charge and discharge strategy of mobile energy storage: one is during 3:00–7:00 when the electricity price is lower, mobile energy storage utilizes grid electricity for charging; the other is during 14:00–16:00 when the load is low and photovoltaics cannot fully integrate, mobile energy storage is charged at the access node. During peak electricity demand periods at 10:00–14:00 and 19:00–22:00, if fixed energy storage cannot effectively regulate the grid voltage, coordinated discharge of mobile and fixed energy storage is implemented to maintain the stable operation of the power system.

6 Conclusion

Energy storage, due to its flexible output and dynamic adjustment characteristics, can provide rich elastic support for the grid, facilitating the efficient integration of large-scale distributed new energy sources and ensuring the stable operation of the grid. This paper proposes a multi-energy storage coordinated optimization strategy that takes into account voltage offset. Initially, a two-layer model is established around the optimal operation cost of Mobile Energy Storage System and Fixed Energy Storage System, as well as minimizing the grid voltage offset. The model is solved and validated using the PSO-GSA algorithm in the IEEE 33-node distribution system, leading to the following conclusions.

(1) In extreme photovoltaic scenarios, based on predicted load data, using the objectives of minimizing operating costs and

minimizing voltage offset, BESS and FESS are optimized in terms of configuration and dispatch. Suitable parameters for energy storage are selected, and mobile energy storage is dispatched to different nodes to provide charging and discharging services. By comparing fixed energy storage with the coordinated operation of fixed and mobile energy storage, and optimizing the configuration and operational strategies of energy storage, the results show that coordinated operation of fixed and mobile energy storage can improve on-site photovoltaic integration while reducing grid voltage offset.

(2) Guiding energy storage systems to participate in the optimal operation of distribution networks through time-of-use electricity prices and time-of-use loads. The strategy involves charging during low demand and discharging during high demand, balancing the demands of both the grid side and the load side. This approach reduces curtailment, minimizes the impact of distributed energy source output instability on the grid, and equips the distribution network with sufficient flexibility to adapt to peak-valley differences, fluctuations, and the growing normality of daily loads.

(3) The mathematical model presented in this paper exhibits multi-dimensional non-linear characteristics. The PSO-GSA hybrid algorithm is employed for model solving, combining the individual optimization of particle swarm algorithm with the local search ability of gravitational search algorithm. This hybrid approach offers better convergence for solving multi-dimensional non-linear problems.

The optimization strategies mentioned in this paper do not consider the impact of different seasons on photovoltaic output, the influence of mobile energy storage routes, and traffic congestion. In future work, these factors, along with the consideration of the impact of different seasons on photovoltaic output, traffic congestion, and the use of smart switches, could be incorporated into the analysis.

Data availability statement

The raw data supporting the conclusion of this article will be made available by the authors, without undue reservation.

Author contributions

LF: Writing–original draft, Writing–review and editing, Conceptualization, Funding acquisition, Supervision. NJ: Writing–original draft, Writing–review and editing, Funding acquisition, Investigation. YZ: Writing–original draft, Writing–review and editing, Funding acquisition, Methodology. ZK: Writing–original draft, Writing–review and editing, Conceptualization, Software. ZQ: Conceptualization, Data curation, Formal Analysis, Funding acquisition, Methodology, Supervision, Validation, Writing–original draft, Writing–review and editing. WS: Writing–original draft, Writing–review and editing, Funding acquisition, Investigation, Methodology.

Funding

Conflict of interest

Authors LF, NJ, and YZ were employed by Nari Group Corporation State.

The remaining authors declare that the research was conducted in the absence of any commercial or financial relationships that could be construed as a potential conflict of interest.

Publisher's note

References

Abdeltawab, H. H., and Mohamed, Y. A.-R. I. (2017). Mobile energy storage scheduling and operation in active distribution systems. *IEEE Trans. Ind. Electron.* 64, 6828–6840. doi:10.1109/TIE.2017.2682779

Anantathanavit, M., and Munlin, M.-A. (2013). "Radius particle swarm optimization," in 2013 International Computer Science and Engineering Conference (ICSEC), Nakorn Pathom, Thailand, September 4-6, 2013 (IEEE), 126–130. doi:10.1109/ICSEC.2013.6694765

Astero, P., Choi, B. J., and Liang, H. (2017). Multi-agent transactive energy management system considering high levels of renewable energy source and electric vehicles. *IET Generation, Transm. Distribution* 11, 3713–3721. doi:10.1049/IET-GTD.2016.1916

Chen, Y., Zheng, Y., Luo, F., Wen, J., and Xu, Z. (2016). Reliability evaluation of distribution systems with mobile energy storage systems. *IET Renew. Power Gener.* 10, 1562–1569. doi:10.1049/iet-rpg.2015.0608

Doraghinejad, M., Nezamabadi-pour, H., Hashempour Sadeghian, A., and Maghfoori, M. (2012). "A hybrid algorithm based on gravitational search algorithm for unimodal optimization," in 2012 2nd International eConference on Computer and Knowledge Engineering (ICCKE), Mashhad, 18-19 October 2012, 129–132. doi:10.1109/ICCKE.2012.6395365

Kwon, S.-Y., Park, J.-Y., and Kim, Y.-J. (2020). Optimal V2G and route scheduling of mobile energy storage devices using a linear transit model to reduce electricity and transportation energy losses. *IEEE Trans. Ind. Appl.* 56, 34–47. doi:10.1109/TIA.2019.2954072

Liu, Z., Yu, P., and Li, J. (2023). Planning of distributed generation and generalized energy storage in distribution network considering operation characteristics. *Dianli Zidonghua Shebei/Electric Power Autom. Equip.* 43, 72–79. doi:10.16081/j.epae.202208029

Lu, Q., Jiang, L., Bie, Z., Zheng, J., Yang, Y., Yu, Z., et al. (2023). Post-disaster fault restoration strategy for distribution network considering optimal scheduling of user-side energy. *Automation Electr. Power Syst.* 47, 44–54. doi:10.7500/AEPS20220226001

Ma, Z., Wei, Z., Chen, S., Zheng, Y., and Wu, T. (2023). Active-reactive power optimal dispatch of AC/DC distribution network based on soft open point. *Automation Electr. Power Syst.* 47, 48–58. doi:10.7500/AEPS20220702002

Mao, M., Liu, Y., Zhang, L., and Zhang, J. (2019). Optimal configuration of generalized energy storage in distribution network with high-penetration renewable energy. *Dianli Xit. Zidonghua/Automation Electr. Power Syst.* 43, 77–85. doi:10.7500/AEPS20180615002

Morstyn, T., Hredzak, B., and Agelidis, V. G. (2018). Control strategies for microgrids with distributed energy storage systems: an overview. *IEEE Trans. Smart Grid* 9, 3652–3666. doi:10.1109/TSG.2016.2637958

Pan, Y., Geng, G., and Jiang, Q. (2023). Consistency algorithm based control strategy for soft open point cluster. *Dianli Xit. Zidonghua/Automation Electr. Power Syst.* 47, 101–109. doi:10.7500/AEPS20211017004

Pasetti, M., Ferrari, P., Bellagente, P., Sisinni, E., de Sá, A. O., Prado, C. B. do, et al. (2021). Artificial neural network-based stealth attack on battery energy storage systems. *IEEE Trans. Smart Grid* 12, 5310–5321. doi:10.1109/TSG.2021.3102833

Shi, M., Xu, K., Wang, J., Yin, R., and Zhang, P. (2021). Short-term photovoltaic power forecast based on grey relational analysis and GeoMAN model. *Trans. China Electrotech. Soc.* 36, 2298–2305. doi:10.19595/j.cnki.1000-6753.tces.200538

Wang, C., Wu, Z., and Li, P. (2014). The prospects and challenges of distributed electricity storage technology. *Automation Electr. Power Syst.* 38, 1–73. doi:10.7500/AEPS20140108002

Wang, S., Liu, Q., Zhao, Q., and Wang, H. (2021). Connotation analysis and prospect of distribution network elasticity. *Automation Electr. Power Syst.* 45, 1–9. doi:10.7500/AEPS20200112006

Wei, C., Li, J., Tu, C., Wang, X., Guo, Q., and Xiao, F. (2023). Optimal regulation and control strategy for flexible interconnected distribution network considering loss characteristics of transformers and soft open points. *Dianli Xit. Zidonghua/Automation Electr. Power Syst.* 47, 69–78. doi:10.7500/AEPS20220915007

Yang, B., Wang, J., Yu, L., Cao, P., Shu, H., and Yu, T. (2022). Peafowl optimization algorithm based Bi-level multi-objective optimal allocation of energy storage systems in distribution network. *Shanghai Jiaot. Daxue Xuebao/Journal Shanghai Jiaot. Univ.* 56, 1294–1307. doi:10.16183/j.cnki.jsjtu.2021.371

Yao, S., Wang, P., Liu, X., Zhang, H., and Zhao, T. (2020). Rolling optimization of mobile energy storage fleets for resilient service restoration. *IEEE Trans. Smart Grid* 11, 1030–1043. doi:10.1109/TSG.2019.2930012

Zhou, N., Fan, W., Liu, N., Lin, X., Zhang, J., and Lei, J. (2016). Battery storage multi-objective optimization for capacity configuration of PV-based microgrid considering demand response. *Dianwang Jishu/Power Syst. Technol.* 40, 1709–1716. doi:10.13335/j.1000-3673.pst.2016.06.015

Nomenclature

Indices

N_I	Equipment type I
C_I	Investment cost of equipment type I
C_I^{loss}	Daily operational maintenance cost of equipment I
G_0	Initial value
P_t^{line}	Power purchased from the grid at time t
w_t^{line}	Electricity price at time t
C_{FUEL}	Unit distance cost

Parameters

D_{PV}	Photovoltaic penetration rate
F_{MAX}	Maximum photovoltaic output power
$F_{L,MAX}$	Maximum load output power
$P_{PV,fact,t}$	Actual generation of photovoltaics at time t
$P_{LOAD,T}$	Distribution network load during the photovoltaic generation period at time t
$P_{ESS,t}$	Load for energy storage charging during the photovoltaic generation period at time t
$P_{i,t}^{MES}$	Injected power at node i by mobile energy storage at time t
E_t^{MES}	State of charge of mobile energy storage at time t
$E_{min}^{MES}, E_{max}^{MES}$	Maximum and minimum values of the state of charge of mobile energy storage
E_0^{MES}, E_T^{MES}	State of charge of mobile energy storage
f_1	Equipment investment costs
f_2	Equipment operating costs
f_3	Grid power purchase cost
f_4	Cost of mobile energy storage migration
P_s	Photovoltaic output power
P_N	Rated power of mobile energy storage
$Q_{s,i}$	Reactive power output at node i due to the power source
$Q_{L,i}$	Reactive power output of the load at node i
C_{first}	Equipment investment cost
Q	Capital recovery factor

Variables

φ	On-site absorption rate of photovoltaic power
α, β	Shape parameters of the Beta distribution
r	Actual solar irradiance during a specific time period
r_{max}	Maximum solar irradiance during that time period
A	Photovoltaic panel area
η	Photovoltaic conversion efficiency
η_c	Charging efficiency of energy storage
η_d	Discharging efficiency of energy storage

w_1、w_2、w_3、w_4	Random number between 0 and 1
q	Annual interest rate
Z	Cost of repairing equipment damage
$O_{DISTANCE}$	Distance traveled by the energy storage vehicle
$P_{ES,j}^{min}$	Lower limit of the charging or discharging power for the jth energy storage unit
$P_{ES,j}(t)$	Charging or discharging power of the jth energy storage unit at time t
$P_{ES,j}^{max}$	Upper limit of the charging or discharging power for the jth energy storage unit
$SOC_j(t)$	State of charge of the energy storage at time t
$P_{t,buy}$	Electricity purchasing power
$\Delta U_{i,t}$	Voltage deviation at time t
$U_{i,t}$	Voltage at node i at time t
$U_{i,min}, U_{i,max}$	Upper and lower limits of node i
$P_{pv,min}$	Minimum output of photovoltaic power
P_{pv}^t	Photovoltaic power output at time t
$P_{pv,max}$	Maximum output of photovoltaic or wind power
$P_{s,i}$	Active power output at node i due to the power source
$P_{L,i}$	Active power output of the load at node i
U_i	Voltage at node i
U_j	Voltage at node j
v_i^t	Velocity of the i th particle at generation t
$pbest_i^t$	The best position of the particle at generation t
x_i^t	The position of the particle at generation t
$gbest$	The best solution
w	Weighted function
c_1	Weighting factor
c_2	Weighting factor
ξ	A constant
∂	Descent coefficient
wv_i^t	Exploration ability of the particle
x_i^{t+1}	Position of particle i at generation t+1
$F_{ij}^d(t)$	Gravitational force of particle i on particle j in the d-dimensional space at the tth iteration
$G(t)$	Value of universal gravitational force at the tth iteration
$M_{pi}(t)$	Active gravitational mass
$M_{aj}(t)$	Passive gravitational mass
$R_{ij}(t)$	Euclidean distance between i and j
$x_j^d(t)$	Position of particle j in the d-dimensional space at the tth generation
$x_i^d(t)$	Position of particle i in the d-dimensional space at the tth generation

$F_i^d(t)$	Total force experienced by individual i in the d-dimensional space at the tth iteration
$a_i^d(t)$	Equation for the acceleration of individual i in the d-dimensional space
$M_i(t)$	Mass of individual i at generation t
$v_i^d(t+1)$	Velocity of particle i in the d-dimensional space at generation t+1
$x_i^d(t+1)$	Position of particle i in the d-dimensional space at generation t+1

| $F_i^d(t)$ | Total force experienced by individual i in the d-dimensional space at the tth iteration |